Calibration of Equivalent Finite Element Model for Packaged Printed Circuit Board by Experimental Modal Analysis

Ying-Chih Lee[1,2], Bor-Tsuen Wang[3], Yi-Shao Lai[1]*, Chang-Lin Yeh[4], Rong-Sheng Chen[2]
[1] Central Labs, Advanced Semiconductor Engineering, Inc., Kaohsiung 811, Taiwan
[2] Department of Engineering Science, National Cheng Kung University, Tainan 701, Taiwan
[3] Department of Mechanical Engineering, National Pingtung University of Science and Technology, Pingtung 912, Taiwan
[4] Shanghai Engineering Center, Advanced Semiconductor Engineering, Inc., Shanghai 201203, China
*Email: yishao_lai@aseglobal.com

Abstract

In this work, the experimental modal analysis (EMA) was performed to establish an equivalent finite element (FE) model for a standard JEDEC drop test printed circuit board (PCB) mounted with packages in a full array. Material properties of the equivalent FE model of the packaged PCB were calibrated through an optimization process with respect to natural frequencies based on EMA results obtained with a free boundary condition. The model was then applied to determine screwing tightness of the packaged PCB corresponding to a fixed boundary condition with the four corners of the PCB constrained, as defined by JEDEC for a board-level drop test.

Introduction

The integrity of solder joints in electronic packages under medium to harsh dynamic loading environments has become a critical issue with the prevalence of portable electronic devices as well as the introduction of stiff and brittle Pb-free solder alloys [1,2]. Several accelerated board-level reliability testing standards aiming at evaluating solder joint reliability that corresponds to these dynamic loading environments, such as cyclic bend [3,4], drop impact [5,6], or vibration [7-12], have been proposed by the Joint Electron Device Engineering Council (JEDEC) [13-16] and have been followed by the industry in qualifying the products.

For the design purpose, the finite element analysis (FEA) has long been proven to be conducive in selecting proper structural configurations and materials for electronic packages without the need of costly and timely experiments. However, the accuracy of numerical solutions depends greatly on the feasibility of modeling that includes proper settings of geometry, boundary and loading conditions, and material properties. For FEA of a board-level test, modeling of the printed circuit board (PCB) is generally considered as the source that brings the most uncertainty to the numerical solutions. Overall mechanical properties of the PCB can vary according to different numbers of metal layers, different layouts of circuits, and different polymeric and composite reinforcing materials used in the fabrication. Tiny circuits and their complex layouts inside the PCB also limit the possibility of comprehensive modeling of the PCB.

We note, however, if the concern is only with overall mechanical properties of the PCB or the board- or system-level test vehicle that contains PCB and packages mounted onto it, an experimental modal analysis (EMA) [17] can practically determine modal parameters, including natural frequencies, mode shapes, and damping ratios, of the specific PCB or board- or system-level test vehicle without the need of prerequisite information of material properties and layouts of its individual constituent components [18-20]. An equivalent finite element (FE) model calibrated by modal parameters obtained from EMA can thus be used with more flexibility for the design purpose [5,21].

In the present work, we followed EMA to characterize modal parameters of a standard 132 mm × 77 mm × 1 mm JEDEC drop test board [13,15] mounted with 13 mm × 13 mm packages in a 3 × 5 full array, as shown in Fig. 1.

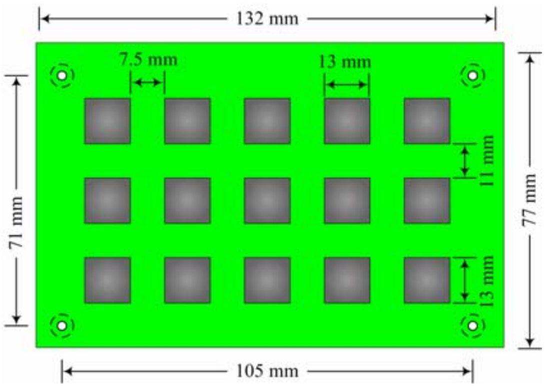

Fig. 1. Schematic of packaged PCB (not to the scale)

The packaged PCB arranged with free and fixed boundary conditions are shown in Fig. 2. Material properties of the equivalent FE model of the packaged PCB were calibrated through an optimization process based on EMA results obtained with a free boundary condition. The model was then applied to determine screwing tightness of the packaged PCB corresponding to a fixed boundary condition with the four corners of the PCB constrained, as defined by JEDEC for a board-level drop test [13,15].

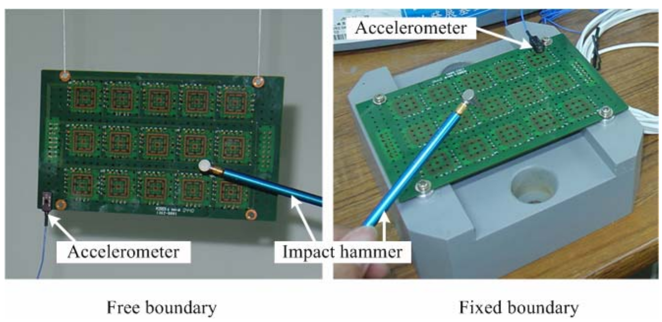

Fig. 2. Packaged PCB with free and fixed boundary conditions (packages on reversed side)

EMA and FEA

Experimental setups for EMA on the packaged PCB with free and fixed boundary conditions have been shown in Fig. 2. To avoid interference, hammering was performed on the reversed side of the packaged surface, Fig. 3, in which the locations where the accelerometer was affixed are labeled.

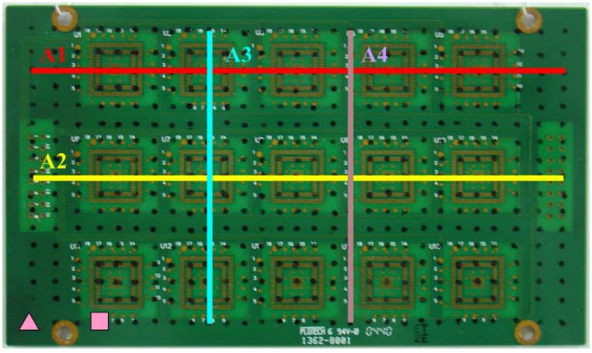

Fig. 3. Grid of measurement points (Accelerometer locations: ▲ for free; ■ for fixed)

For the free boundary condition, we measured hammering force and acceleration responses corresponding to hammering locations in a 17 (vertical) × 29 (horizontal) array on the surface, shown by the black dots in Fig. 3. For the fixed boundary condition, hammering force and acceleration responses corresponding to 88 hammering locations along the A1 through A4 lines shown in Fig. 3 were measured. The frequency response functions (FRFs) between measured hammering force and acceleration responses were then curve-fitted to extract experimental modal parameters of the packaged PCB.

Fig. 4 shows full three-dimensional FE models built for the packaged PCB with free and fixed boundary conditions. The model for the packaged PCB contained 12,335 linear hexahedral solid elements along with 24 mass elements to take into account the accelerometer mass. For the fixed boundary condition, 192 additional linear spring-damper elements were employed to account for the tightness of screws at the four corners. The damping effect of the screws was neglected in this study while only the spring effect was considered. The spring constant was assumed to be constant and was to be determined in the subsequent optimization procedure after the material properties of the packaged PCB were determined from the optimization based on EMA and FEA results for the free boundary condition.

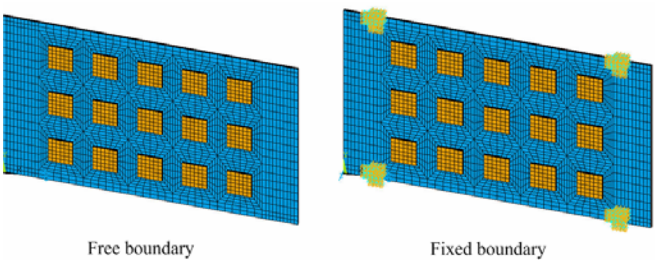

Fig. 4. FE models of packaged PCB

Initial material properties extracted from Yeh and Lai [22], listed in Table 1, were specified to PCB and packages. We assume that the packages are isotropic while the PCB is cubic with three independent elastic constants, albeit isotropy was given to the PCB as an initial setting. The accelerometer mass is 1.5 g.

Table 1. Initial material properties of packaged PCB [22]

	PCB	Package
Young's modulus (GPa)	15.50	28.00
Poisson's ratio	0.20	0.35
Mass density (g/cm^3)	1.91	1.81

A numerical convergence analysis based on the initial material properties was carried out with respect to natural frequencies of the first five modes of the packaged PCB, as shown in Table 2. Clearly from the results, the FE model with 12,335 elements has achieved sufficient accuracy with moderate computational efficiency.

Table 2. Convergence analysis with respect to natural frequencies (Unit: Hz)

Cell / Mode	A	B	C	D	B vs. C
	Number of elements				
	3,620	7,245	12,335	17,415	Relative error (%)
1	178.97	148.91	147.34	145.48	1.054
2	220.50	191.13	189.46	188.12	0.875
3	465.73	393.58	386.87	385.85	1.705
4	491.95	394.27	391.00	388.19	0.829
5	495.89	401.51	395.20	388.39	1.572
6	772.80	562.22	551.21	549.91	1.958

An optimization process based on the coincidence of numerical and experimental natural frequencies was followed to iterate material properties as well as the spring constant of the packaged PCB. For the free boundary condition, design variables include Young's modulus (E_b), shear modulus (G_b), Poisson's ratio (ν_b), and mass density (ρ_b) of the PCB as well as Young's modulus (E_p), Poisson's ratio (ν_p), and mass density (ρ_p) of the packages. The design variables were than iteratively optimized with respect to the minimal sum of square errors between numerical and experimental natural frequencies and the criterion was set at a relative error within 10%. After the optimal material properties were obtained for the packaged PCB using results corresponding to the free boundary condition, the spring constant was then solely determined following the same optimization process based on numerical and experimental natural frequencies corresponding to the fixed boundary condition.

Free Boundary Condition

For the free boundary condition, we measured hammering force and acceleration responses corresponding to 493 hammering locations on the surface of the packaged PCB. Hammering was performed three times at each of the 493 locations. Experimental FRFs corresponding to individual hammering locations were curve-fitted using ME'scope VES v. 3.0 (Vibrant Technology, Inc., Scotts Valley, CA, USA) to obtain experimental modal parameters of the packaged PCB, whose material properties were then optimized with respect to natural frequencies and listed in Table 3. The measure of anisotropy of the PCB is $2G_b(1+\nu_b)/E_b = 82.8\%$ with the optimized material properties. Our study also showed that no eligible correlation could be obtained in this case when the PCB was assumed to be isotropic.

Table 3. Comparison between initial and optimized material properties of packaged PCB

	Initial	Optimized	Discrepancy (%)
E_b (GPa)	15.50	9.42	39.2
G_b (GPa)	6.46	3.12	51.6
ν_b	0.20	0.25	25.0
ρ_b (g/cm^3)	1.91	2.05	6.8
E_p (GPa)	28.00	20.00	28.6
ν_p	0.35	0.4	14.3
ρ_p (g/cm^3)	1.81	1.84	1.6

We denote a pair (*i*,*j*) in which *i* stands for the output signal location, *i.e.*, the accelerometer location and *j* stands for the input signal location, *i.e.*, the hammering location. In the present case, the accelerometer located close to the 465th hammering point. Fig. 5 shows two examples of FRFs up to 2 kHz and corresponding coherence functions for (465,180) and (465,465), for which the latter indicates that the hammering location is right beside the accelerometer.

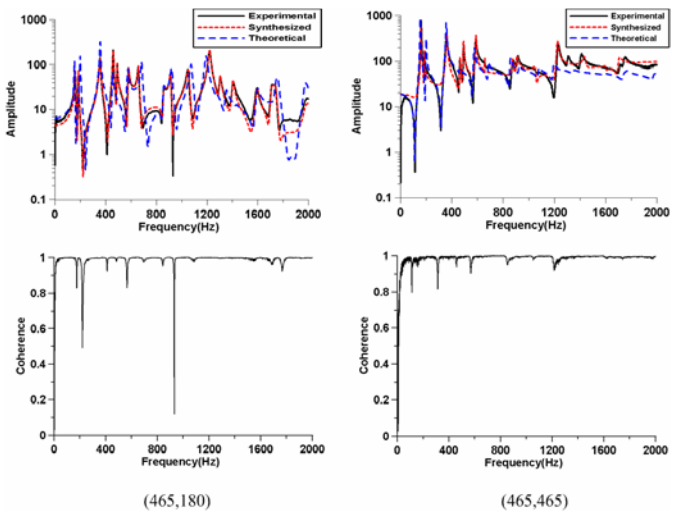

Fig. 5. Representative FRFs and corresponding coherence functions for packaged PCB with free boundary condition

In the figure, the synthesized curve refers to the FRF after curve-fitting while the theoretical curve represents the FE solution based on the optimized material properties. From the figure we note that measured and numerical FRFs are in reasonably good agreement. Moreover, the coherence functions approach unity up to 2 kHz except at the frequencies where anti-resonance occurs, indicating that at each hammering location, the three hammerings generated consistent results and hence the experiments were reliable.

To further verify the equivalent FE model with the optimized material properties, we compare its natural frequencies and corresponding mode shapes up to 2 kHz with EMA results using the mode assurance criterion (MAC) [17], defined by

$$\mathrm{MAC}\left(\{\phi_x\},\{\phi_p\}\right)=\frac{\left|\{\phi_x\}^T\{\phi_p^*\}\right|^2}{\{\phi_x\}^T\{\phi_x^*\}\{\phi_p\}^T\{\phi_p^*\}}, \qquad (1)$$

to quantitatively evaluate the discrepancy between measured mode shape, $\{\phi_x\}$, and predicted mode shape, $\{\phi_p\}$. The asterisk in Eq. (1) denotes the conjugate. For two coincident mode shapes, MAC = 1.

We note that there are 18 modes up to 2 kHz for the packaged PCB with the free boundary condition. Table 4 shows, for instance, the first eight modes. In the table, E_n and F_n refer to EMA and FEA results, respectively, for the *n*-th mode. Modal characteristics along longitudinal and lateral directions are shown in parenthesis.

Table 4. Natural frequencies and corresponding mode shapes for packaged PCB with free boundary condition

Mode	Frequency (Hz) / Discrepancy (%)	EMA	FEA	MAC / (m,n)
E_1 vs. F_1	161 vs. 154 / 4.3	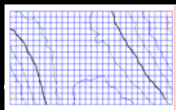	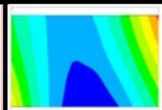	0.91 / (3,1)
E_2 vs. F_2	187 vs. 200 / 7.0	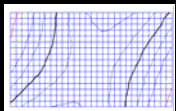		0.83 / (3,1)
E_3 vs. F_3	356 vs. 357 / 0.3	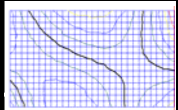	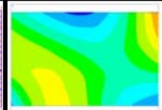	0.91 / (3,2)
E_4 vs. F_4	461 vs. 457 / 0.9	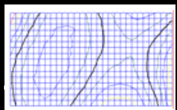	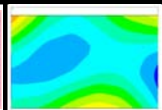	0.68 / (4,1)
E_5 vs. F_5	492 vs. 467 / 5.1	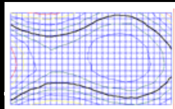		0.70 / (1,3)
E_6 vs. F_6	582 vs. 574 / 1.4	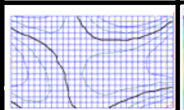	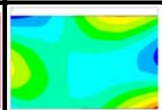	0.97 / (2,3)
E_7 vs. F_7	660 vs. 684 / 3.6	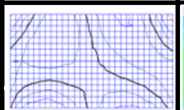	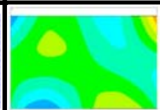	0.97 / (4,2)
E_8 vs. F_8	858 vs. 857 / 1.2	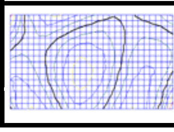	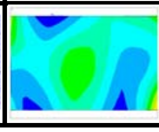	0.97 / (5,1)

The comparison of the 18 modes up to 2 kHz indicates that natural frequencies obtained by EMA and FEA are in good agreement with discrepancies within 7%. Mode shapes from EMA and FEA also agree very well with each other with MACs greater than 0.9 except for only a few modes whose MACs are small.

Fixed Boundary Condition

Following the same grid numbering as in the case of the free boundary condition, the accelerometer in the case of the fixed boundary condition located close to the 468th point. Representative FRFs for (468,74) and (468,358) up to 2 kHz are shown in Fig. 6.

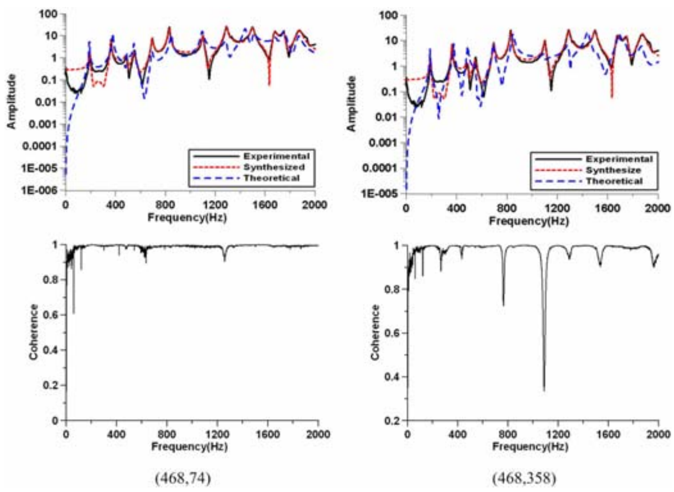

Fig. 6. Representative FRFs and corresponding coherence functions for packaged PCB with fixed boundary condition

Clearly, measured and numerical FRFs are in reasonably good agreement while the coherence functions approach the unity except at the frequencies where anti-resonance occurs. With the optimized material properties, the spring constant for the packaged PCB with the fixed boundary condition was determined as 2.78 MN/m through the optimization process.

We note that there are 15 modes up to 2 kHz for the packaged PCB with the fixed boundary condition. Table 5, for instance, summarizes and compares natural frequencies and corresponding mode shapes of the first eight modes obtained by EMA and FEA. The comparison of mode shapes is shown along lines A1 through A4 because hammering was performed along these lines only to speed up the experiment. The comparison of the 15 modes up to 2 kHz indicates that natural frequencies obtained by EMA and FEA are in very good agreement with discrepancies less than 2%. Mode shapes from EMA and FEA also agree very well with each other with MACs greater than 0.9 except for only a few modes whose MACs are small.

Modal Damping Ratios

Modal damping ratios can only be obtained from experimental measurements. In Table 6 we show modal and accumulated average damping ratios for the packaged PCB with free and fixed boundary conditions. The accumulated average damping ratio is defined by $\bar{\xi} = \sum_{i=1}^{n} \xi_i / n$, where ξ_i represents the damping ratio of the i-th mode. From the table we note that in general a higher mode has a smaller damping ratio.

Table 5. Natural frequencies and corresponding mode shapes for packaged PCB with fixed boundary condition

Mode	Frequency (Hz) / Discrepancy (%)	EMA	FEA	MAC / (m,n)
E_1 vs. F_1	194 vs. 192 / 1.3	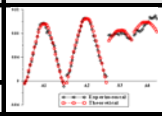	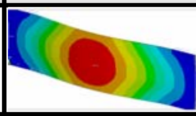	0.99 / (1,1)
E_2 vs. F_2	364 vs. 380 / 4.3	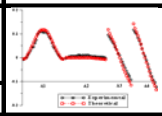	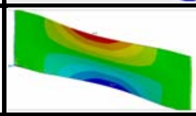	0.99 / (1,2)
E_3 vs. F_3	487 vs. 491 / 0.9	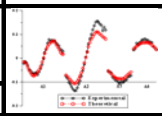	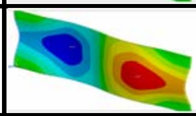	0.96 / (2,1)
E_4 vs. F_4	549 vs. 553 / 0.7	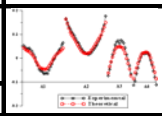	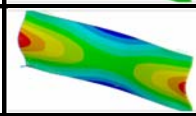	0.95 / (3,3)
E_5 vs. F_5	695 vs. 696 / 0.1	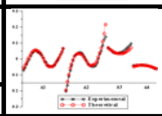	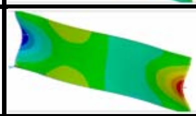	0.94 / (4,1)
E_6 vs. F_6	833 vs. 850 / 2.0	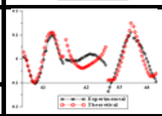	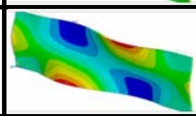	0.66 / (4,2)
E_7 vs. F_7	845 vs. 860 / 1.7	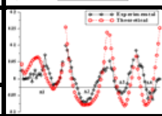	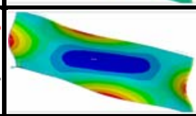	0.84 / (3,3)
E_8 vs. F_8	1100 vs. 1100 / 0.0	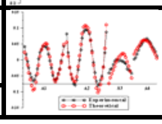	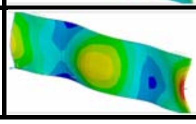	0.93 / (5,1)

Table 6. Modal damping ratios of packaged PCB (%)

Mode	Free boundary		Fixed boundary	
	Experimental	Accumulated average	Experimental	Accumulated average
E_1	2.250	2.250	1.432	1.432
E_2	0.673	2.139	0.698	1.065
E_3	1.350	1.358	1.693	1.379
E_4	0.580	1.339	1.658	1.519
E_5	0.511	1.139	0.777	1.148
E_6	0.706	1.001	0.772	0.960
E_7	0.647	0.951	3.153	2.056
E_8	0.861	0.904	0.574	1.315
E_9	0.569	0.896	0.707	1.011
E_{10}	0.739	0.857	0.888	0.949
E_{11}	0.690	0.844	0.865	0.907
E_{12}	0.532	0.828	0.668	0.788
E_{13}	0.576	0.803	0.759	0.773
E_{14}	0.771	0.784	0.928	0.851
E_{15}	0.587	0.782		
E_{16}	0.611	0.769		
E_{17}	1.260	0.758		

These damping ratios are beneficial to the transient analysis of the packaged PCB that follows the concept of modal superposition [23,24].

Conclusions

An equivalent FE model for a standard 132 mm × 77 mm × 1 mm JEDEC drop test PCB mounted with 13 mm × 13 mm packages in a 3 × 5 full array has been established based on EMA results corresponding to free and fixed boundary conditions. Natural frequencies and mode shapes obtained by EMA and FEA are generally in very good agreement. We also provide modal damping ratios obtained experimentally, which would benefit the transient analysis of the packaged PCB that follows the concept of modal superposition.

As a concluding remark, we have demonstrated in this work that overall material properties and screwing tightness of a packaged PCB can be determined by incorporating EMA and FEA along with an optimization process. This technique is conducive to the FE modeling of complex PCB structures for the design for mechanical reliability.

References

1. Wong, E. H. *et al*, "Drop Impact: Fundamentals and Impact Characterisation of Solder Joints," *Proc. 55th Electron. Compon. Technol. Conf.*, Lake Buena Vista, FL, USA, 2005, pp. 1202-1209.
2. Lai, Y.-S. *et al*, "Evaluation of Solder Joint Strengths Under Ball Impact Test," *Microelectron. Reliab.*, Vol. 47, No. 12 (2007), pp. 2179-2187.
3. Mercado, L. L. *et al*, "Handheld Use Condition-Based Bend Test Development," *IEEE Trans. Adv. Packag.*, Vol. 29, No. 2 (2006), pp. 240-249.
4. Lai, Y.-S. *et al*, "Cyclic Bending Reliability of Wafer-level Chip-Scale Packages," *Microelectron. Reliab.*, Vol. 47, No. 1 (2007), pp. 111-117.
5. Lai, Y.-S. *et al*, "Experimental Studies of Board-level Reliability of Chip-Scale Packages Subjected to JEDEC Drop Test Condition," *Microelectron. Reliab.*, Vol. 46, No. 2-4 (2006), pp. 645-650.
6. Chong, D. Y. R. *et al*, "Drop Impact Reliability Testing for Lead-free and Lead-based Soldered IC Packages," *Microelectron. Reliab.*, Vol. 46, No. 7 (2006), pp. 1160-1171.
7. Yang, Q. J. *et al*, "Vibration Reliability Characterization of PBGA Assemblies," *Microelectron. Reliab.*, Vol. 40, No. 7 (2000), pp. 1097-1107.
8. Wang, H. *et al*, "Vibration Fatigue Experiments of SMT Solder Joint," *Microelectron. Reliab.*, Vol. 44, No. 7 (2004), pp. 1143-1156.
9. Kim, Y. *et al*, "Vibration Fatigue Reliability of BGA-IC Package with Pb-free Solder and Pb-Sn Solder," *Microelectron. Reliab.*, Vol. 46, No. 2-4 (2006), pp. 459-466.
10. Liu, X. *et al*, "Experimental Study and Life Prediction on High Cycle Vibration Fatigue in BGA Packages," *Microelectron. Reliab.*, Vol. 46, No. 7 (2006), pp. 1128-1138.
11. Gu, J. *et al*, "Prognostics Implementation of Electronics Under Vibration Loading," *Microelectron. Reliab.*, Vol. 47, No. 12 (2007), pp. 1849-1856.
12. Chen, Y. S. *et al*, "Combining Vibration Test with Finite Element Analysis for the Fatigue Life Estimation of PBGA Components," *Microelectron. Reliab.*, Vol. 48, No. 4 (2008), pp. 638-644.
13. JEDEC Solid State Technology Association, JESD22-B110: Subassembly Mechanical Shock, 2001.
14. JEDEC Solid State Technology Association, JESD22-B103-B: Vibration, Variable Frequency, 2002.
15. JEDEC Solid State Technology Association, JESD22-B111: Board Level Drop Test Method of Component for Handheld Electronics Products, 2003.
16. JEDEC Solid State Technology Association, JESD22-B113: Board Level Cyclic Bend Test Method for Interconnect Reliability Characterization of Components for Handheld Electronic Products, 2006.
17. Ewins, D. J., Modal Testing: Theory, Practice and Application, 2nd Ed., Research Studies Press (Baldock, Hertfordshire, UK, 2000).
18. Yang, Q. J. *et al*, "Experimental Modal Analysis of PBGA Printed Circuit Board Assemblies," *Proc. 1st Electron. Packag. Technol. Conf.*, Singapore, 1997, pp. 290-296.
19. Gibson, R. F., "Modal Vibration Response Measurements for Characterization of Composite Materials and Structures," *Composites Sci. Technol.*, Vol. 60, No. 15 (2000), pp. 2769-2780.
20. He, X. and Fulton, R., "Modeling and Simulation of the Dynamic Response of the Electronic Packaging," *Proc. 50th Electron. Compon. Technol. Conf.*, Las Vegas, NV, USA, 2000, pp. 1535-1547.
21. Pitarresi, J. *et al*, "Dynamic Modeling and Measurement of Personal Computer Motherboards," *Proc. 52nd Electron. Compon. Technol. Conf.*, San Diego, CA, USA, 2002, pp. 597-603.
22. Yeh, C.-L. and Lai, Y.-S., "Support Excitation Scheme for Transient Analysis of JEDEC Board-level Drop Test," *Microelectron. Reliab.*, Vol. 46, No. 2-4 (2006), pp. 626-636.
23. Tsai, T.-Y. *et al*, "Response Spectra Analysis for Undamped Structural Systems Subjected to Half-Sine Impact Acceleration Pulses," *Microelectron. Reliab.*, Vol. 47, No. 8 (2007), pp. 1239-1245.
24. Yeh, C.-L. *et al*, "Transient Analysis of Drop Responses of Electronic Packages Using Response Spectra Incorporated with Modal Superposition," *Microelectron. Reliab.*, Vol. 47, No. 12 (2007), pp. 2188-2196.